Investigating the delay between dust radiation and star-formation in local and distant quenching galaxies

Laure Ciesla, Veronique Buat, Mederic Boquien, Alessandro Boselli, David Elbaz, Gregoire Aufort

A&A 653, A6 (2021)
https://doi.org/10.1051/0004-6361/202140762

Astronomy & Astrophysics

Investigating the delay between dust radiation and star-formation in local and distant quenching galaxies

L. Ciesla[1], V. Buat[1,2], M. Boquien[3], A. Boselli[1], D. Elbaz[4], and G. Aufort[1]

[1] Aix-Marseille Université, CNRS, LAM (Laboratoire d'Astrophysique de Marseille) UMR7326, 13388 Marseille, France
e-mail: laure.ciesla@lam.fr
[2] Institut Universitaire de France (IUF), Paris, France
[3] Centro de Astronomía (CITEVA), Universidad de Antofagasta, Avenida Angamos 601, Antofagasta, Chile
[4] AIM-Paris-Saclay, CEA/DSM/Irfu - CNRS – Université Paris Diderot, CEA-Saclay, Pt Courrier 131, 91191 Gif-sur-Yvette, France

Received 9 March 2021 / Accepted 27 May 2021

ABSTRACT

We investigate the timescale over which the infrared (IR) luminosity decreases after a complete and rapid quenching of star formation using observations of local and high-redshift galaxies. From spectral energy distribution modelling, we derive the time since quenching of a subsample of 14 galaxies from the *Herschel* Reference Survey that suffer from ram-pressure stripping due to the environment of the Virgo cluster and of a subsample of 7 rapidly quenched COSMOS galaxies selected through a state-of-the-art statistical method already tested on the determination of galaxy star formation history (SFH). Three out of the seven COSMOS galaxies have an optical spectrum with no emission line, confirming their quenched nature. We obtained the present physical properties of the combined sample (local plus high-redshift) from the long-term SFH properties, as well as the past $L_{\rm IR}$ of these galaxies just before their quenching. We show that this past $L_{\rm IR}$ is consistent with the $L_{\rm IR}$ of reference samples of normally star-forming galaxies with same stellar mass and redshift as each of our quenched galaxies. We put constraints on the present to past IR luminosity ratio as a function of quenching time. The two samples probe different dynamical ranges in terms of quenching age with the HRS galaxies exhibiting longer timescales (0.2–3 Gyr) compared to the COSMOS ones (<100 Myr). Assuming an exponential decrease in the $L_{\rm IR}$ after quenching, the COSMOS quenched galaxies are consistent with short e-folding times of less than a couple of hundred million years, while the properties of the HRS quenched galaxies are compatible with larger timescales of several hundred million years. For the HRS sample, this result is consistent with the known quenching mechanism that affected them, namely ram pressure stripping due to the environment. For the COSMOS sample, different quenching processes are acting on short to intermediate timescales. Processes such as galaxy mergers, disk instabilities, and environmental effects can produce such strong star formation variability.

Key words. galaxies: evolution – galaxies: fundamental parameters

1. Introduction

The infrared (IR) luminosity of a galaxy is a key parameter that is tightly linked to its star formation activity and can be directly converted to determine its star formation rate (SFR, e.g., Kennicutt & Evans 2012). Although most of the time the true SFR of a galaxy agrees well with the SFR inferred from the IR luminosity for galaxies actively forming stars, there are some evolutionary phases when the two are discrepant (Hayward et al. 2014; Boquien et al. 2014). This is the case when galaxies experience short-term variations of their star formation history (SFH) such as rapid quenching. As a consequence, when using the IR luminosity as an SFR indicator one can conclude that a particular galaxy is still forming stars even when star formation has, in reality, recently been quenched (Hayward et al. 2014). This bias may have significant consequences when investigating the short-term SFH of galaxies in the context of the star-forming main sequence (MS) paradigm (Elbaz et al. 2007; Noeske et al. 2007), for instance. The main consequence of this tight relation between SFR and the stellar mass of galaxies is that they are forming the bulk of their stars through steady-state processes rather than violent episodes of star formation.

Although the MS is found to hold up to $z = 4$ (Schreiber et al. 2017) with little variation of its normalisation or shape with redshift (Daddi et al. 2007; Pannella et al. 2009; Elbaz et al. 2011; Rodighiero et al. 2011; Speagle et al. 2014; Whitaker et al. 2014; Schreiber et al. 2015; Gavazzi et al. 2015; Tomczak et al. 2016), what is striking is that the scatter of the MS is found to be relatively constant at all masses and over cosmic time (Guo et al. 2013; Ilbert et al. 2015; Schreiber et al. 2015). Several studies have found a coherent variation of physical galaxy properties such as gas fraction (Magdis et al. 2012), Sersic index, effective radius (Wuyts et al. 2011), and U-V color (e.g., Salmi et al. 2012), suggesting that the bulk of the scatter is related to physics and not measurement and model uncertainties. From an observational point of view, Elbaz et al. (2018) showed that some massive compact galaxies exhibiting starburst galaxy properties (short depletion time and high IR surface density) can be found within the MS. However, these have a different morphology and gas fraction compared to 'true' starbursts (above the MS), indicating a different origin, possibly being late-stage mergers of gas-rich galaxies. This could be the sign of a possible recent movement of these galaxies from the starburst galaxy region back to the MS. From a theoretical perspective, oscillations of the SFR resulting from a varying infall rate and compaction of star formation have also been advocated to explain the MS scatter (e.g., Dekel & Burkert 2014; Sargent et al. 2014; Scoville et al. 2016; Tacchella et al. 2016). These variations

must be small enough to keep the SFR of the galaxy within the MS scatter. However, based on EAGLE simulations, Matthee & Schaye (2019) showed that although individual galaxies can cross the MS multiple times during their evolution, the main tracks around which they oscillate are linked to their halo properties; that is, galaxies above or below the MS at $z = 0.1$ tend to have been above or below the MS, respectively, for more than 1 Gyr. Using 150 zoom-in simulations of galaxies, Blank et al. (2021) obtained consistent results. Therefore, there is no consensus on the evolution of galaxies relative to the MS and accurate measurements of the positions of galaxies, present and past, on the SFR–M_* diagram are needed in order to shed light on their short-term evolution.

As a step towards this goal, we aim, in the present work, to put constraints on the timescales over which the IR luminosity decreases after a complete shutdown of star formation activity. To do so, we recover the past IR luminosity of our studied galaxies, just before quenching, from broad band spectral energy distribution (SED) modelling, as well as their past star-forming properties. Here, the word 'quenching' is used to reflect rapid quenching processes that take place on timescales of less than ~1 Gyr as opposed to slower mechanisms such as mass quenching for instance.

The paper is organised as follows: In Sects. 2–4, we describe the *Herschel* Reference Survey (HRS, Boselli et al. 2010b) local sample, the broad band SED modelling method, and the selection of rapidly quenched candidates among the HRS, respectively. To extend our study in terms of luminosity and redshift, we select a complementary sample of rapidly quenched galaxies from the COSMOS survey in Sect. 5. The evolution of the IR luminosity of both the local and high-redshift samples is presented in Sect. 6 and discussed in Sect. 7. Finally, our conclusions are provided in Sect. 8. Throughout this paper, we assume the Salpeter (1955) IMF.

2. The sample of local galaxies

We use the HRS which is a combined volume- and flux-limited sample composed of local galaxies at distances of between 15 and 25 Mpc. The galaxies are selected according to their K-band magnitude, a reliable proxy for the total stellar mass (Gavazzi et al. 1996). The sample contains 322[1] galaxies, among which 62 early-type and 260 late-type. We refer the reader to Boselli et al. (2010b) for additional information on the sample. In this work we only consider the 260 late-type galaxies.

The HRS sample is well suited for this study; it is partly composed of sources that are part of the Virgo cluster. Entering the intracluster medium, these galaxies have their gas content stripped through ram pressure stripping, which is quantified through a deficit of HI gas content, resulting in quenching of their star formation activity on a timescale ranging from a few hundred million years to a couple of gigayears (see e.g., Boselli et al. 2016). As we aim to study the decrease in IR luminosity after the shutdown of star formation, these sources are good targets. Furthermore, the wealth of both photometric and spectroscopic ancillary data available for the HRS galaxies is an asset and allows us to probe the SFH of the galaxies as well as their IR properties (Bendo et al. 2012; Cortese et al. 2012, 2014; Ciesla et al. 2012, 2014; Boselli et al. 2013, 2014a, 2015, and from the literature). The photometric bands used in this work are listed in Table 1. A sample of high-redshift galaxies complementing the HRS local sample is described in Sect. 5.

[1] With respect to the original sample given in Boselli et al. (2010b), the galaxy HRS 228 is removed from the complete sample because its updated redshift on NED indicates it as a background object.

Table 1. HRS broad band set of filters.

Telescope/Camera	Filter name	$\lambda_{\rm mean}$(μm)	Ref.
GALEX	FUV	0.153	a
	NUV	0.231	a
	U	0.365	b
	B	0.44	b
SDSS	g	0.475	a
	V	0.55	b
SDSS	*r*	0.622	a
SDSS	*i*	0.763	a
2MASS	*J*	1.25	b
	H	1.65	b
	Ks	2.1	b
Spitzer	IRAC1	3.6	c
	IRAC2	4.5	c
	IRAC4	8	d
WISE	3	12	d
	4	22	d
Spitzer	MIPS1	24	e
	MIPS2	70	e
Herschel	PACS green	100	f
	PACS red	160	f
	PSW	250	g
	PMW	350	g
	PLW	500	g

References. [(a)]Cortese et al. (2012). [(b)]Compilation from the literature, details are provided in Boselli et al. (2010b). [(c)]S^{4}G: Querejeta et al. (2015). [(d)]Ciesla et al. (2014). [(e)]Bendo et al. (2012). [(f)]Cortese et al. (2014). [(g)]Ciesla et al. (2012).

3. Spectral energy distribution modelling

3.1. The CIGALE code

We use the SED modelling and fitting code CIGALE[2] (Boquien et al. 2019), which is used to model and fit the UV to submillimetre (submm) emission of galaxies assuming an energy balance between the emission absorbed by dust in UV–optical and that re-emitted in IR. It is a versatile code composed of modules that model the SFH, the stellar emission, the dust emission, the active galactic nucleus (AGN) contribution, and the radio emission of galaxies. In CIGALE, the SFH can be handled through analytical functions or using simulated SFHs (Boquien et al. 2014; Ciesla et al. 2015, 2017).

In a previous study, we investigated the use of simple analytical SFH forms to recover galaxy parameters (Ciesla et al. 2015). A set of SFHs from semi-analytical models with known associated properties (SFR, M_*, etc.) were used to test different SFH analytical forms to recover them (one or two exponentially declining SFHs, and a delayed SFH used in this paper). The delayed SFH can recover the SFR and M_* properties associated to these simulated SFHs even in bursty SFHs (see for instance Fig. 7 of Ciesla et al. 2015). More recently, in Ciesla et al. (2017) we studied the possibility to recover the same properties in cases where galaxies recently experienced strong variations. For these sources, the addition of an extra flexibility in the recent SFH is needed to better recover the SFR. This was further confirmed by

[2] http://cigale.lam.fr

Aufort et al. (2020) from a statistical approach. As in this paper we are only focusing on the latest SFH variation, we rely on these studies and use a delayed SFH associated with the recent flexibility, as presented and described in Ciesla et al. (2017) and Aufort et al. (2020). The delayed-τ SFH is defined as:

$$\mathrm{SFR}(t) \propto t \times \exp(-t/\tau_{\mathrm{main}}), \quad (1)$$

where SFR is the star formation rate, t the time, and τ_{main} is the e-folding time. The flexible SFH is an extension of the delayed-τ model:

$$\mathrm{SFR}(t) \propto \begin{cases} t \times \exp(-t/\tau_{\mathrm{main}}), & \text{when } t \leq t_{\mathrm{flex}} \\ r_{\mathrm{SFR}} \times \mathrm{SFR}(t = t_{\mathrm{flex}}), & \text{when } t > t_{\mathrm{flex}}, \end{cases} \quad (2)$$

where t_{flex} is the time at which the star formation is instantaneously affected, and r_{SFR} is the ratio between $\mathrm{SFR}(t > t_{\mathrm{flex}})$ and $\mathrm{SFR}(t = t_{\mathrm{flex}})$:

$$r_{\mathrm{SFR}} = \frac{\mathrm{SFR}(t > t_{\mathrm{flex}})}{\mathrm{SFR}(t_{\mathrm{flex}})}. \quad (3)$$

From this we can define $\mathrm{age}_{\mathrm{flex}}$ which is the age of the galaxy minus t_{flex}. As we focus on quenched galaxies for the rest of the study, we refer to $\mathrm{age}_{\mathrm{flex}}$ as $\mathrm{age}_{\mathrm{trunc}}$, the age of the SFH truncation, for clarity. In addition to the flexible delayed-τ SFH, the SEDs of our sample are fitted using the stellar population models of Bruzual & Charlot (2003), the Charlot & Fall (2000) attenuation recipe, and the Dale et al. (2014) dust emission models.

The goal of this paper is to recover the past and present properties of a sample of galaxies. However, the attenuation curve of the galaxies before and after the quenching is probably different, and the dust content and dust–star geometry should vary as well. We choose to use the Charlot & Fall (2000) attenuation law where a different attenuation is assumed for young ($<10^7$ years) and old ($>10^7$ years) stars. Light from both young and old stars is attenuated by the interstellar medium (ISM) but the emission from young stars is also affected by the dust in the birth clouds (BCs). Both of these forms of attenuation are modelled by power laws with n_{ISM} and n_{BC}. Furthermore, there is a μ parameter defined as $\mu = A_V^{\mathrm{ISM}}/(A_V^{\mathrm{ISM}} + A_V^{\mathrm{BC}})$ that can be used to handle the attenuation of old and young populations and thus change the effective attenuation law (e.g., Battisti et al. 2020). The difference in dust geometry is therefore handled through this parameter. The A_V^{ISM} parameter is free in our SED fitting procedure, but ,$_{\mathrm{ISM}}$, n_{BC}, and μ are fixed to −0.7, −0.7, and 0.3, respectively. We tested several runs of SED fitting whilst varying these three parameters: (n_{ISM}, n_{BC}, μ) combinations of (−0,7; −0.7; 0.3), (−1; −1; 0.3), and (−0.7, −1.3; 0.3), and the same combinations with μ variable (0.2, 0.3, 0.4). For each test and for the quenched candidates, we compared the quality of the new fit to the one proposed in our paper using the Bayesian information criterion (see e.g., Ciesla et al. 2018; Aufort et al. 2020). The fits with different combinations did not result in a better quality fit than the one adopted here. Varying μ did not result in a better fit of the data despite the additional degree of freedom. However, we note that the Charlot & Fall (2000) attenuation law intrinsically takes into account some variations in the attenuation curves with time due to stellar populations ages. The input parameters used for each module are provided in Table 2.

3.2. The SED fitting procedure

To reach the goal of this study, that is to put constraints on the decrease in IR luminosity after rapid quenching of star formation, we perform the SED fitting in two steps. First, we model the whole SED of the 260 star-forming galaxies of the HRS from UV to submm. This run allows us to estimate the age at which a recent variation of the SFH, if needed, occurred. We then reconstruct the SFH of the galaxies to estimate the IR luminosity of the galaxies immediately before the recent variation of SFH, a procedure that we explain in detail in Sect. 6. In a second step, we fit only the IR part of the SED with data from MIPS 24 µm to *Herschel*/SPIRE 500 µm in order to obtain a measurement of the current IR luminosity independently from the UV–near-infrared(NIR) SED of the galaxy.

Table 2. Input parameters used in the SED fitting procedures with CIGALE.

Parameter	Value
Flexible delayed-τ SFH	
age (Gyr)	11, 11.5, 12, 12.5, 13
τ_{main} (Gyr)	[2; 17], 5 values linearly sampled
$\mathrm{age}_{\mathrm{trunc}}$ (Myr)	[10; 3000], 30 values log-sampled
r_{SFR}	[10^{-3}; 10^{2}], 20 values log-sampled
Dust attenuation: Charlot & Fall (2000)	
A_V ISM	[0.2; 2.2], 15 values linearly sampled
μ	0.3
n_{ISM}	−0.7
$n_{\mathrm{Birth\,Cloud}}$	−0.7
Dust emission: Dale et al. (2014)	
α	1.5, 2.0, 2.5

3.3. Constraints on the parameters

Before analysing the results from SED fitting, we need to confirm that the measured parameters are indeed constrained by the data. To do this, we perform a mock analysis with CIGALE, a functionality available in the code. The procedure is explained in Giovannoli et al. (2011) and Boquien et al. (2019) for example; here, we summarise the main steps. A first run is made with CIGALE from which we obtain the best model for each galaxy and the corresponding physical properties (stellar mass, SFR, age, etc.). The best SED model of each galaxy, for which we know all parameters, is integrated into the same set of filters as our observed sample. These mock flux densities are then perturbed by adding a noise randomly selected in a Gaussian distribution with a σ corresponding to the error of the original flux density. CIGALE, in the same configuration, is then run on this new mock catalogue for which each parameter is known. The mock analysis then consists in comparing the results of the Bayesian-like analysis provided by CIGALE for this mock catalogue to the input parameters used to build it. If there is a one-to-one relationship between the input and output values of a parameter then it is perfectly constrained by the data in hand. We use this test to check the robustness of the output SED fitting parameters, our ability to constrain them, and the possible degeneracies that can arise.

The results of the mock analysis performed on our HRS sample are shown in Fig. 1 (grey symbols). The stellar mass is well constrained which is expected because there is good coverage of the NIR wavelength range. Overall SFRs are well recovered which is also expected because our sample benefits from a good UV-to-IR coverage (Buat et al. 2014), with the exception of a couple of sources. For the same reason, the V band attenuation parameter, A_V, is also well estimated.

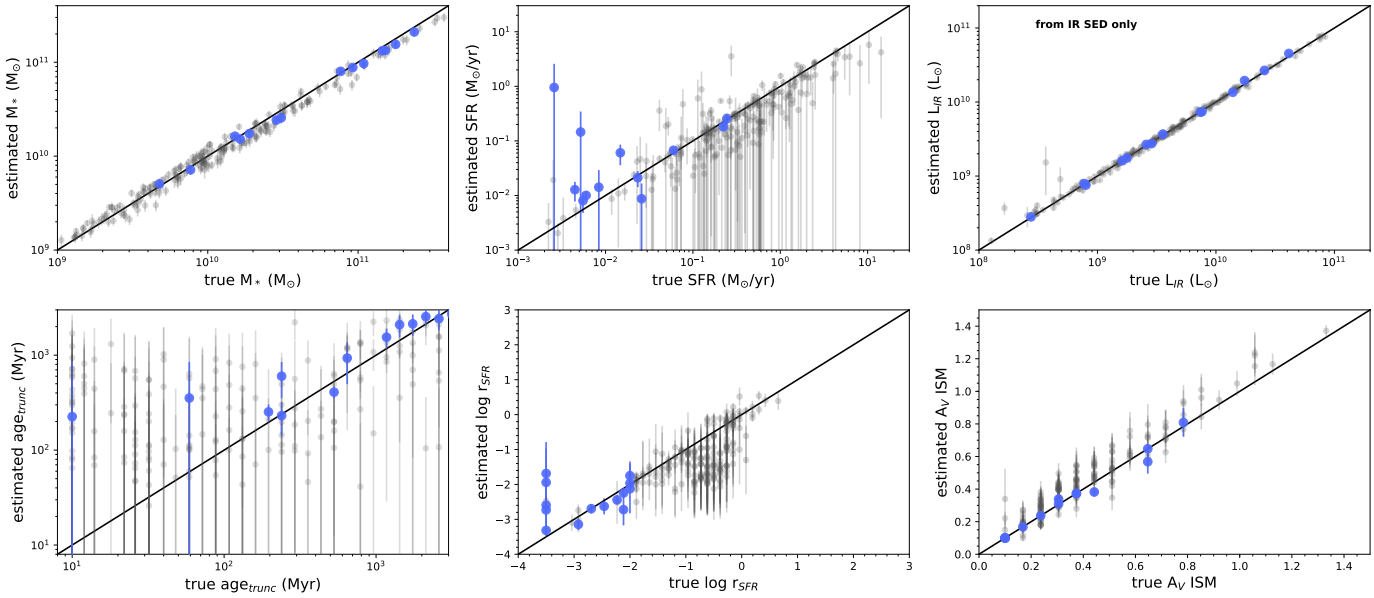

Fig. 1. Results of the mock analysis. The input parameters used to build the mock catalogue are shown on the *x*-axis while the results of the fitting of the mock catalogues are shown on the *y*-axis. A good constraint on a given parameter is obtained when there is a one-to-one relationship, which is indicated by the black solid lines. Grey dots are all HRS galaxies while blue circles are the galaxies selected as rapidly quenched.

Regarding the parameters linked to the SFH, we find that $\tau_{\rm main}$ is not well constrained, showing a dispersed relation, as discussed in previous studies (e.g., Buat et al. 2014; Ciesla et al. 2016). For the $r_{\rm SFR}$ parameter, the relation between the input value and the one recovered by CIGALE does not follow an exact one-to-one relationship. Indeed, at the lowest and highest input values, the relation is flat. The lowest input values are overestimated, and the highest values are underestimated. This could be due to a well-known effect of PDF analysis: the value estimated from the Bayesian-like analysis comes from the probability distribution function (PDF) of the parameter. The final value is the mean of the PDF while the error is its standard deviation. However, for the extreme values (lowest and highest) this PDF is truncated and therefore the mean value is skewed toward higher parameter values and lower parameter values for the lowest and highest input parameter values, respectively (e.g., Noll et al. 2009; Buat et al. 2012; Ciesla et al. 2015). Furthermore, values between 0.1 and 1 tend to be underestimated. Another possibility is that for very low values of $r_{\rm SFR}$ the spectrum of the galaxy does not show a lot of variation and becomes insensitive to the parameter, and therefore the PDF becomes flat. In the following, we discuss how we choose our selection criteria to minimise the biases linked to the difficulty in constraining $r_{\rm SFR}$. We note that for most of the galaxies, the $r_{\rm SFR}$ seems to be underestimated by a factor of about ten. We take this into account while defining our selection criteria in the following.

Finally, the age$_{\rm trunc}$ parameter shows a dispersed distribution for the whole sample. This is not surprising as the majority of the HRS galaxies are normal star-forming galaxies with a quasi constant SFH over the last several gigayears. Therefore, for these galaxies the truncated SFH is not well-suited; hence the difficulty to constrain age$_{\rm trunc}$. The same problem could be at the origin of the difficulty in constraining $r_{\rm SFR}$ as well for normal galaxies. However, we show in the following that age$_{\rm trunc}$ is well recovered for quenched galaxies.

The IR luminosity obtained from the fit of the IR SED only is very well constrained and is recovered by the SED fitting, which is not surprising given the good IR coverage.

4. A fiducial sample of local quenched galaxies

4.1. Selection of HRS quenched galaxies

We choose to apply a cut in $r_{\rm SFR}$ to select galaxies that are close to being totally quenched. Based on the mock analysis described in the previous section, by selecting galaxies with $r_{\rm SFR} \leq 0.01$, that is sources for which the SFR after quenching is lower by a factor larger than 100, we ensure a conservative sample. Indeed, as shown in Fig. 1 (lower middle panel, blue dots) candidates with $r_{\rm SFR} \leq 0.01$ show better agreement between the input and output values of the mock with the exception of the very low values of $r_{\rm SFR}$ that tend to be overestimated but still in the range of our criteria. In addition to a selection from $r_{\rm SFR}$, we impose that the galaxies must have more that one detection in IR to ensure a reliable $L_{\rm IR}$ estimate from the IR SED.

With these two criteria, the final local sample of quenched galaxies is composed of 14 galaxies. These galaxies are marked by the blue dots in Fig. 1. For these galaxies, the age$_{\rm trunc}$ is very well constrained with all the points lying close to the one-to-one relationship, with the exception of the two galaxies with the shortest input quenching age, which tends to be overestimated. This could be due to the known bias from the PDF analysis described above. In any case, for these two galaxies the error on the quenching age is large and is taken into account in our analysis. The SFR of the quenched candidates is well constrained except for the two sources mentioned above that have an overestimated quenching age. All the other physical properties of this quenched sample are well constrained according to the mock analysis.

These 14 galaxies are Virgo cluster members known to undergo ram pressure stripping. This process removes the gas efficiently, especially in the outer parts of the disk, truncating the star formation activity outside-in (Boselli et al. 2006, 2016). The lack of both atomic and molecular gas (Fumagalli et al. 2009; Boselli et al. 2014b) reduces the star formation activity, yielding a migration of the galaxies from the blue cloud to the green valley and then the red sequence as predicted in models (Boselli et al. 2006, 2016). However, there have been cases of Jellyfish

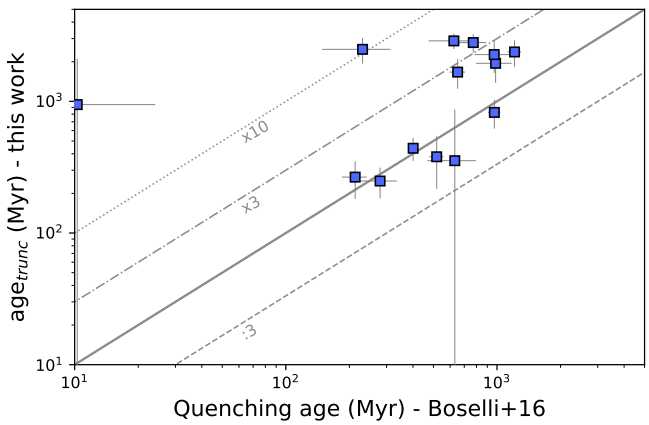

Fig. 2. Comparison between the age of quenching estimated in this work from broad band photometry and the same age estimated by Boselli et al. (2016) from a combination of spectroscopic and photometric data. The solid line shows the one-to-one relationship.

galaxies showing some enhancement of star formation despite undergoing ram pressure (Durret et al. 2021). These galaxies have been selected in B or V optical bands from their Jellyfish morphology. They thus show an intermediate-age stellar population in their morphological tails by selection. Ram pressure stripping only affects gas, not stars, and therefore it is probable that these galaxies underwent some gravitational interactions too, capable of removing stars as well as gas. An increase in star formation due to ram pressure is only possible in the case of an almost edge-on interaction of a galaxy into the intracluster medium: the gas moves towards the disk before being removed from the galaxy, this leads to compression of the gas and therefore a burst of star formation as observed in IC3476 (Boselli et al. 2021). This burst is relatively short –as the stripping process is rapid (<500 Myr)– and is thus statistically difficult to observe. Based on these arguments, we are confident that our selected HRS galaxies are indeed quenched due to ram pressure stripping, in agreement with observations and model predictions of this process.

4.2. Comparison with the results from Boselli et al. (2016)

Using galaxies from the HRS sample, Boselli et al. (2016) aimed to constrain the rapid decrease in star formation activity of galaxies entering the dense environment of the Virgo cluster. To do so, these authors combined UV to far-IR photometric data with age-sensitive Balmer absorption line indices extracted from medium-resolution ($R \sim 1000$) integrated spectroscopy, as well as Hα imaging data. They use CIGALE, combining all of their data and using a truncated SFH with a secular evolution parametrised using the chemo-spectrophotometric physically justified models of Boissier & Prantzos (2000).

Given the combination of spectroscopic (Balmer lines, including Hα) and photometric data (20 bands from UV to submm) and tailored SFHs, the results of Boselli et al. (2016) are a reference and benchmark for ours. From their SED modelling, these latter authors obtained an estimate of the quenching age (QA) of their galaxies. The QA is the lookback time of the epoch of the quenching episode, which has the same definition as the age$_{\rm trunc}$ parameter used in this work. The two quantities can therefore be directly compared.

To understand whether or not our method, using only broad-band photometry, allows us to recover sensible estimates of the age of quenching, in Fig. 2 we show a comparison of our estimate of age$_{\rm trunc}$ and the QA parameter of Boselli et al. (2016). Even though the relationship is dispersed, the same order of age, that is within a factor of three, is found for 10 out of the 14 galaxies. Two galaxies are in strong disagreement with Boselli et al. (2016), with our method estimating a quenching age of between a factor ten and higher than Boselli et al. (2016). One of these two galaxies is found to give a very short quenching age by Boselli et al. (2016) (<20 Myr) whereas our method does not provide a good constraint on the value. Considering the difficulty in estimating SFH parameters from broad-band SED fitting (e.g., Pforr et al. 2012; Buat et al. 2014; Ciesla et al. 2015, 2016), the different attenuation law that we use, and the good agreement –within a factor of three– between the estimate of Boselli et al. (2016) using spectroscopy information plus photometry and ours, we consider that our method does not introduce a strong bias in the quenching age determination.

5. A complementary sample of $0.5 < z < 1$ COSMOS quenched galaxies.

The HRS sample is well-suited for our study as we have all the information needed regarding their UV to submm SED and the star formation quenching mechanism at play. However, it is a particular sample of galaxies at $z = 0$ lying within the Virgo cluster. Furthermore, the dynamical range probed by the HRS galaxies is relatively limited in terms of luminosity. We now want to understand if other galaxies follow the same relation or if the decrease in IR luminosity after quenching depends on other factors. In the following, we make a first attempt to identify sources at higher redshift that could be used to complete our study, that is, galaxies that very recently underwent a drastic and rapid decrease in their star formation activity, to be compared with the HRS selected galaxies. A well-suited sample for this study is the COSMOS sample as it provides both a large wavelength coverage of the SED and the large statistics needed to pinpoint objects showing a rapid variation of their SFH.

5.1. COSMOS subsample and results from Aufort et al. (2020)

To select the high-redshift galaxy sample, we rely on the results of Aufort et al. (2020) who aimed to identify galaxies having experienced a rapid and drastic variation of their star formation activity in the last 500 Myr from a sample of COSMOS galaxies (Laigle et al. 2016) with good-quality data S/N >10. These authors selected a sample of galaxies from the COSMOS sample with $0.5 < z < 1$, stellar mass larger than $10^{8.5}$ $M_\odot$, and high-S/N flux densities. They developed a method based on approximate Bayesian computation (ABC; see, e.g., Marin et al. 2012; Sisson et al. 2018) combined with a machine-learning algorithm (XGBoost, see Chen & Guestrin 2016) to compute the probability that a galaxy experienced a recent (less than 500 Myr) and drastic variation of its star formation activity that could be either an enhancement of the SFR or quenching. Based on the observed SED of a galaxy, Aufort et al. (2020) chose the most appropriate SFH between a finite set. The main idea behind ABC is to rely on many simulated SEDs generated from all the SFHs in competition using parameters drawn from the prior. For each of the galaxies of their sample, the posterior probability p that a galaxy has experienced a recent and rapid variation of star formation activity is computed. We rely on this probability to select our

Table 3. COSMOS broad and intermediate bands used in this work.

Instrument	Band	λ (µm)	# of sources	# final
GALEX	FUV	0.153	331	5
GALEX	NUV	0.229	376	7
CFHT	u'	0.355	376	7
SUBARU	B	0.443	376	7
SUBARU	V	0.544	376	7
SUBARU	r	0.622	376	7
Suprime Cam	i'	0.767	376	7
Suprime Cam	z'	0.902	376	7
Intermediate bands		0.427	376	7
”		0.464	376	7
”		0.505	376	7
”		0.527	376	7
”		0.574	376	7
”		0.624	376	7
”		0.709	376	7
”		0.738	376	7
”		0.767	376	7
”		0.827	376	7
HSC	Y		376	7
VISTA	Y	1.019	376	7
VISTA	J	1.250	376	7
VISTA	H	1.639	376	7
VISTA	Ks	2.142	376	7
Spitzer	IRAC1	3.6	376	7
Spitzer	IRAC2	4.5	376	7
Spitzer	IRAC3	5.8	300	5
Spitzer	IRAC4	8.0	179	1
Spitzer	MIPS	24	194	4
Herschel	PACS	100	53	0
Herschel	PACS	160	40	0
Herschel	SPIRE	250	42	1
Herschel	SPIRE	350	18	1

Notes. The data up to *Spitzer*/IRAC4 are from Laigle et al. (2016) while the IR data are from Jin et al. (2018). The number of sources with a detection in each band is provided in the last two columns for the whole sample and the selected quenched sources.

galaxies and conservatively select those with $p > 0.91$ which corresponds to galaxies where there is ‘very strong’ to ‘decisive’ evidence for a recent strong variation of the SFH according to the Jeffreys scale (see, e.g., Robert 2007). Of the 12 380 galaxies of their sample, 376 galaxies have a posterior probability higher than 0.91.

Although the results of Aufort et al. (2020) allow us to select galaxies with a recent variation of SFH, their method does not provide information on the nature of this variation, that is, whether a galaxy underwent a starburst phase or a quenching of SF. For the purpose of this study, we need to select galaxies that underwent a strong decrease in SFR. Therefore, we combine UV and IR data of our COSMOS subsample of 376 galaxies from the catalogues of Laigle et al. (2016) and Jin et al. (2018) to determine the nature of the variation from SED modelling. We include the intermediate bands as well as all the *Spitzer*/IRAC ones. We use the Jin et al. (2018) IR COSMOS catalogue from 24 µm to 350 µm (no detection is found at longer wavelengths for the 376 galaxies). In IR, we only consider detection with an S/N larger than 3. The list of bands used in this study is provided in Table 3 along with the number of detections in each of them.

5.2. Constraints on the parameters for the COSMOS selected galaxies

As for the HRS galaxies, we proceed to a mock analysis to understand how well the output parameters from the fit are constrained. Indeed, given the redshift of the SED as well as the different photometric bands used compared to HRS, the results obtained for the local galaxies are not necessarily applicable in the case of the COSMOS galaxies. The results of the mock analysis performed on our sample of 376 galaxies are shown in Fig. 3. Similarly to the HRS galaxies, the stellar mass, SFR, $L_{\rm IR}$, and A_V ISM attenuation are well constrained.

Regarding the parameters linked to the SFH, the relation between the input value and the one recovered by CIGALE of the $r_{\rm SFR}$ parameter does not follow an exact one-to-one relationship for the same reason as explained above for the HRS galaxies (bias due to the PDF analysis). Nevertheless, this known bias is not a strong issue for our analysis. Indeed, as seen from Fig. 3, the recovered $r_{\rm SFR}$ values from input $\log r_{\rm SFR} < 0$ remain below zero. This means that selecting galaxies with a negative value of $\log r_{\rm SFR}$ is a conservative approach as this value can be slightly overestimated because of the PDF analysis performed by CIGALE.

The $\rm age_{trunc}$ parameter shows a more dispersed relation between the input and output values with large uncertainties. However, as we discuss in the following section, the selection criteria that we apply allow us to be relatively confident about the estimate of $\rm age_{trunc}$ of our quenched candidates.

5.3. Selection of recently quenched galaxies

To separate galaxies having experienced a recent starburst from those that were recently quenched, we ran CIGALE on the 376 galaxies that have a probability higher than 91% according to Aufort et al. (2020). The input parameters used in CIGALE are the same as those used for the mock analysis and are provided in Table 2. However, to limit degeneracies, we used an option of CIGALE which is the possibility to provide parameters to be fitted in the same way as any other photometric flux density. We therefore assume an age of the COSMOS galaxies based on their redshift, and use this as an input to be fitted by the code. Therefore, it is not a fixed parameter but a strong constraint for the SED fit. This reasonable assumption allows us to reduce the free parameters of the SFH modelling from four to three.

To be conservative, we apply to the COSMOS galaxies the same selection criterion as for the HRS local sample, that is $r_{\rm SFR} \leq 0.01$. Of the 376 galaxies of our sample, 7 satisfy this criterion.

The constraints on the parameters obtained from SED fitting for these sources are shown in Fig. 3 in blue. The SFR of these galaxies is more uncertain and slightly overestimated compared to the other galaxies of the full sample of 376 sources, which is not surprising given their low star formation activity. The bias in the extreme values of the mock analysis may also play a role in this. However, as explained in Sect. 3.3, our selection is conservative as the actual $r_{\rm SFR}$, and therefore SFR values, may be lower than what is estimated by CIGALE. Regarding the age of quenching, $\rm age_{trunc}$, the PDF analysis of the parameter can lead to overestimation of the true value by a factor of four at most. The $\rm age_{trunc}$ of quenched candidates with an estimated $\rm age_{trunc}$ lower than 50 Myr are constrained because the output age resulting from the mock analysis is also below 50 Myr. Although we are using broad-band SED fitting to estimate variations of SFH on very short timescales (<100 Myr), the UV rest-frame data are

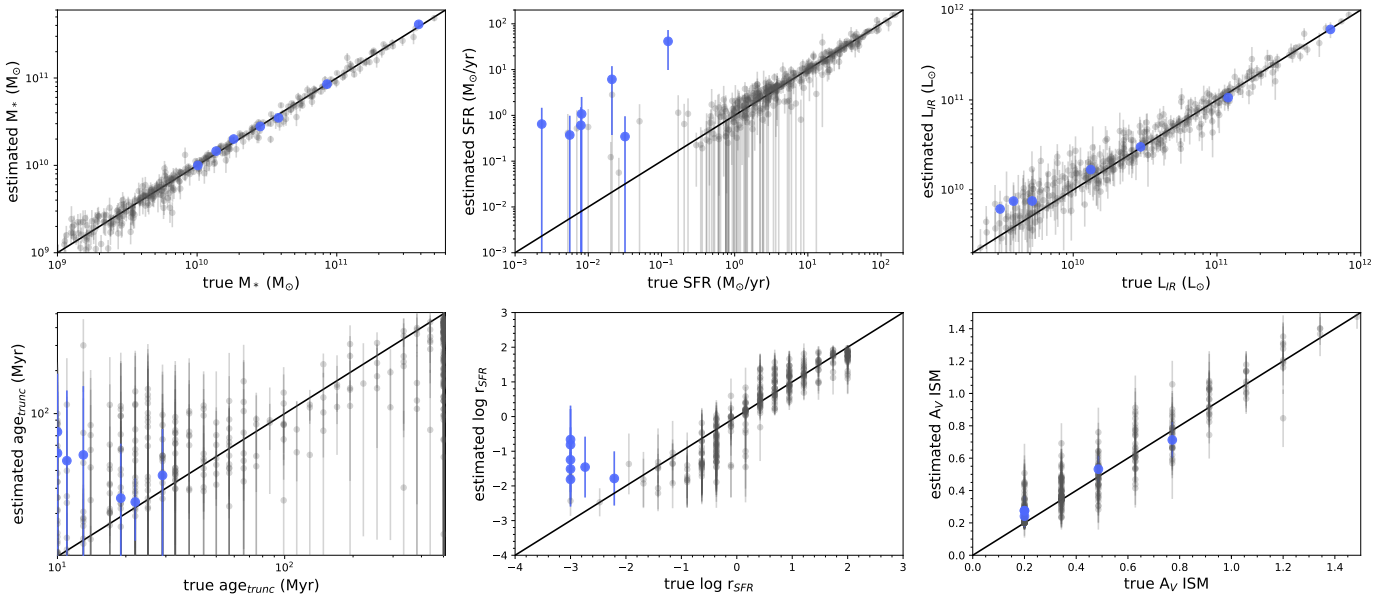

Fig. 3. Results of the mock analysis. The input parameters used to build the mock catalogue are shown on the *x*-axis while the results of the fitting of the mock catalogues are shown on the *y*-axis. A good constraint on a given parameter is obtained when there is a one-to-one relationship, which is indicated by the black solid lines. Grey dots are all sources selected from the Aufort et al. (2020) sample while blue circles are the galaxies composing the final sample.

sufficiently sensitive to be able to probe these scales with SED fitting as demonstrated by Boquien et al. (2014) using hydrodynamical simulations of MS galaxies. Despite the large errors, we can still obtain information about the $\mathrm{age_{trunc}}$ which remains short (<100 Myr).

As a sanity check, we ran CIGALE on these seven galaxies using only a normal delayed-τ SFH and compared the quality of the fits provided by the two models (normal delayed-τ and flexible SFH). As their SFR is very low, we want to be sure that their SED could not be fitted by a normal delayed-τ SFH with low values of τ_{main} (<3 Gyr) which is usually assumed to model passive and quiescent galaxies. To this end, we computed the Bayesian information criterion (BIC) for each SFH assumption and calculated the difference between them, that is ΔBIC (see Ciesla et al. 2018; Buat et al. 2019; Aufort et al. 2020, for more details). For the seven galaxies of our final sample, ΔBIC is larger than ten, which is the threshold above which we can claim that the evidence against a normal delayed-τ SFH is decisive (see, e.g., Robert 2007). This strengthens the results of the Aufort et al. (2020) method in selecting galaxies with a recent and strong variation of SFH and ensures that our sample is not contaminated by passive or smoothly quenched galaxies.

To confirm that our selection yields a sample of quenched galaxies, we searched for optical spectra for all seven. We find three galaxies with a zCOSMOS (Lilly et al. 2009) optical spectra, which we retrieved from the ASPIC[3] database, shown in Appendix A. The optical spectra of the three galaxies show no strong emission lines that could suggest star formation activity, indicating that $\mathrm{age_{trunc}}$ is larger than 10 Myr, the typical age of HII regions. These three sources are therefore confirmed to be quenched and serve as fiducial indicators in the following.

Of the 12 380 galaxies from the sample of Aufort et al. (2020), we select seven galaxies. However, we cannot deduce any statistical information from this number on the population of galaxies undergoing rapid quenching. Indeed, first of all, in the selection of their sample, Aufort et al. (2020) adopted some criteria to keep the statistical problem simple, such as an S/N cut and a detection of the galaxies in all the main photometric bands they used. Therefore their sample is not complete. Furthermore, as the present study is a first attempt at recovering the past recent properties of galaxies undergoing a rapid quenching of their SF, we are very conservative in our criteria in order to have a clean sample. Here, again, our selection does not provide a complete subsample of recently quenched galaxies.

5.4. Physical properties of the selected quenched galaxies

Examples of the fits obtained by CIGALE for the three spectroscopically confirmed quenched galaxies are shown in Fig. 4. The stellar masses, IR luminosities, attenuation (A_V), and quenching ages of each of the seven candidates are shown in Table 4.

In our final sample, only four of the galaxies have an IR detection. To check the validity of the L_{IR} estimate by CIGALE in the absence of such a measurement for the three remaining galaxies, we compare in Fig. 5 the L_{IR} obtained by CIGALE with and without using the available MIPS 24 µm flux density. For this test, we use galaxies of the initial sample of 376 sources that are detected in MIPS 24 µm. There is a relatively good one-to-one relationship between the two measurements, especially because here we consider galaxies that have either undergone a star-bursting event or quenching of their star formation activity, that is, galaxies outside the galaxy star-forming MS. This is consistent with the results of Małek et al. (2018) who performed the same test on a large sample of IR galaxies from HELP[4] (*Herschel* Extragalactic Legacy Project Vaccari 2016) and found a significant relation between the IR luminosity estimates with and without using the IR data. This relation allows us to consider that the L_{IR} estimated by CIGALE in the absence of IR data is a fair approximation of the true L_{IR} of the galaxy; we use this L_{IR} in the remainder of the paper.

[3] http://cesam.lam.fr/aspic/

[4] https://herschel.sussex.ac.uk/

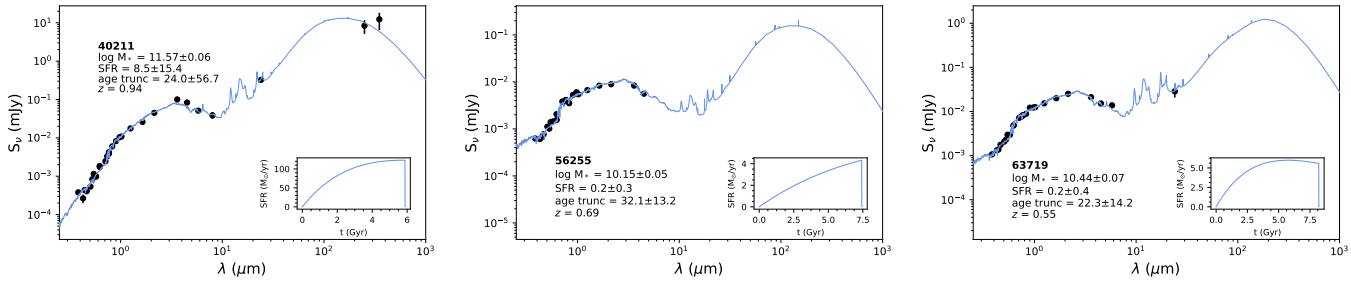

Fig. 4. Examples of SEDs of galaxies from the final COSMOS quenched sample fitted with CIGALE. The black dots are the data points while the blue solid lines indicate the best-fit model. The inset panels show the SFH obtained from the best fit. Key physical parameters are provided for each galaxy. These three galaxies are those confirmed as quenched from their optical spectra.

Table 4. Physical properties obtained with CIGALE for the seven quenched candidates of the final high-z sample.

ID	Redshift	$10^{10}\,M_*$ ($M_\odot$)	$10^9 L_{\rm IR}$ ($L_\odot$)	A_V	Age$_{\rm trunc}$	Optical spectra	MIPS detected
5043	0.63	1.01 ± 0.08	7.5 ± 5.6	0.34 ± 0.13	42 ± 89	NO	NO
40211	0.94	37.34 ± 2.41	603.2 ± 77.9	2.15 ± 0.14	24 ± 57	YES	YES
43190	0.59	3.76 ± 0.38	30.3 ± 4.7	0.75 ± 0.11	49 ± 99	NO	YES
51525	0.74	8.37 ± 0.81	122.7 ± 15.1	2.11 ± 0.14	54 ± 94	NO	NO
56255	0.69	1.40 ± 0.07	4.5 ± 1.2	0.21 ± 0.03	32 ± 13	YES	NO
63719	0.55	2.74 ± 0.18	15.2 ± 3.0	0.53 ± 0.08	22 ± 14	YES	YES
74332	0.53	1.87 ± 0.09	6.0 ± 1.9	0.21 ± 0.04	25 ± 8	NO	NO

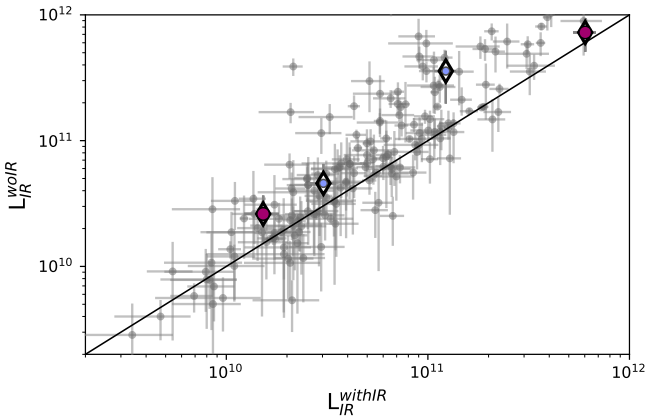

Fig. 5. Comparison between the $L_{\rm IR}$ obtained by CIGALE from UV–IR SED modelling with and without using the MIPS 24 μm flux density for galaxies that are MIPS detected. Candidates of the final sample with a MIPS 24 μm detection are indicated by diamonds. Red circles indicate the candidates of the final sample for which the quenching is confirmed by spectroscopy.

6. The evolution of IR luminosity after quenching

We now combine the local and high-redshift samples. As discussed above, directly from the modelling of the UV-submm SED, we have an estimate of the time at which the quenching of star formation happened, age$_{\rm trunc}$. From the fit of the IR SED, we measured the $L_{\rm IR}$ at the time the galaxy is observed. To investigate the evolution of the IR luminosity after the shutdown of the star formation activity, we need to estimate the IR luminosity just before the quenching as a reference to quantify the decrease since the quenching. We therefore need to recover the past star formation activity of our quenched candidates as traced by the $L_{\rm IR}$. To obtain such an estimate for each galaxy of the joined sample (HRS+COSMOS), we use the SFH best-fit parameters of the observed UV-submm SED and build the SED immediately before quenching. Specifically, we use the long-term SFH parameters ($\tau_{\rm main}$ and age). By building the past SED, we determine the $L_{\rm IR}$ at the time immediately before quenching, which we call $L_{\rm IR}^{\rm bq}$, i.e. 'before quenching'.

According to the hypothesis driven by our SFH model, our quenched candidates are supposed to have been forming stars before this star formation activity was abruptly quenched. If this is indeed the case, then the recovered past IR luminosity, $L_{\rm IR}^{\rm bq}$, should be consistent on average with the $L_{\rm IR}$ of a reference sample of normal star-forming galaxies with the same stellar mass[5]. For each local and high-redshift candidate, we built a reference sample of galaxies with stellar masses of between 0.8 and 1.2 times the stellar mass of the candidate and computed the median $L_{\rm IR}$ of this reference sample, $L_{\rm IR}^{\rm ref}$. For the HRS quenched galaxies, the bins are drawn from the whole sample of 260 late-type HRS galaxies, and using only the IR SED fit. For the COSMOS quenched galaxies, the bins are drawn from the whole initial sample of Aufort et al. (2020) of 12 380 galaxies, and using only the $L_{\rm IR}$ obtained from the UV-submm SED fit, as we showed that it provides a good estimate of the true $L_{\rm IR}$ even with sparse IR sampling of the SED.

In Fig. 6, we show the $L_{\rm IR}^{\rm bq}$ of each of the HRS and COSMOS quenched galaxies as a function of their corresponding $L_{\rm IR}^{\rm ref}$. Six out of the seven COSMOS galaxies are lying very close to the one-to-one relationship. We checked that the large error on age$_{\rm trunc}$ for four of the seven galaxies of COSMOS does not impact the estimate of $L_{\rm IR}^{\rm bq}$ by varying age$_{\rm trunc}$ within the error and found that our measurement is stable. For the COSMOS sources, we are able to use broad-band SED fitting to recover the $L_{\rm IR}$ before the quenching of star formation. This may be due to the fact that these COSMOS galaxies quenched recently, that is, less than 100 Myr ago according to our estimate of age$_{\rm trunc}$.

[5] We checked that the quenching does not significantly affect the stellar mass of the galaxies.

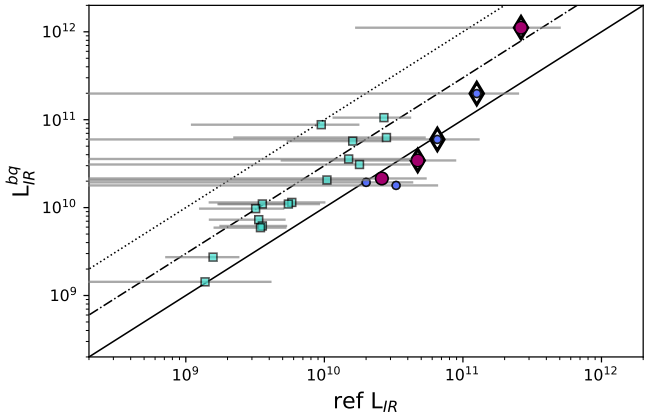

Fig. 6. Estimated $L_{\rm IR}$ of the sources before quenching as a function of the median $L_{\rm IR}$ of a reference sample with similar stellar mass. The cyan squares are the HRS quenched galaxies while the dots are the COSMOS ones. COSMOS galaxies with a diamond are sources with a 24 µm detection. Red dots are COSMOS quenched galaxies that are spectroscopically confirmed. The error bars show the dispersion of the $L_{\rm IR}$ distribution of each reference sample. The solid line shows the one-to-one relationship while the dashed-dotted and dotted lines show a factor three and a factor ten above it, respectively.

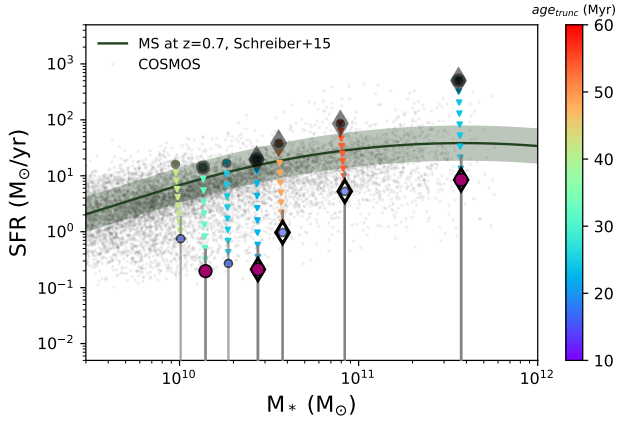

Fig. 7. Star formation rate as a function of stellar mass for the COSMOS galaxies. Grey dots are the whole COSMOS subsample of Aufort et al. (2020). Blue dots, red dots, and diamonds are the seven COSMOS quenched sources studies in this work; their position relative to the star-forming MS of galaxies before their quenching is marked by grey symbols and their evolution since quenching is indicated by the triangles coloured according to their $\rm age_{trunc}$. For comparison, the MS of Schreiber et al. (2015) at $z \sim 0.7$ is shown as a solid black line along with its dispersion (shaded grey region).

However, for one galaxy (#40211) the $L_{\rm IR}^{\rm bq}$ seems to be larger than the corresponding $L_{\rm IR}^{\rm ref}$ by a factor of approximately three. This galaxy benefits from good data as it has been detected in 24µm and its quenching is confirmed from optical spectroscopy. Given the fact that our method provides good estimates of the $L_{\rm IR}$ before quenching for the six other COSMOS sources, the discrepancy between the $L_{\rm IR}^{\rm bq}$ of #40211 and its corresponding $L_{\rm IR}^{\rm ref}$ could be interpreted as a possible indication that this galaxy was experiencing a star-bursting phase just before quenching, hence the high $L_{\rm IR}^{\rm bq}$. Following a similar approach to that used by Ciesla et al. (2018), we show in Fig. 7 the present and past positions of the seven COSMOS quenched sources on the MS diagram. Six out of the seven are compatible with lying on or close to the MS before their quenching. The seventh source, #40211, seems to have been in a star-bursting phase before undergoing a decrease in star formation activity as discussed immediately above. This diagram indicates the relatively short timescale on which the COSMOS galaxies have departed from the MS, providing tentative indications as to the movements of galaxies within the MS. This is consistent with the tight scatter observed in the MS that implies that variations of star formation activity happen on relatively short timescales (e.g., Förster Schreiber & Wuyts 2020, and references therein).

Regarding the HRS quenched galaxies, 11 out of the 14 candidates have $L_{\rm IR}^{\rm bq}$ and $L_{\rm IR}^{\rm ref}$ consistent within a factor of between one and three. For these galaxies, the probed $\rm age_{trunc}$ are longer with values of between 300 Myr and 3 Gyr. These longer timescales make recovery of the past SED more challenging. The HRS is a well-known galaxy sample for which a wealth of ancillary data and studies are available and we know that in this case the slight overestimation of the $L_{\rm IR}^{\rm bq}$ is probably not due to a past star-bursting phase. However, although the members of this sample do not lie exactly on the one-to-one relationship, our method is able to recover the IR luminosity, and thus the star formation properties, of the galaxies within a factor of three on timescales of a few hundred million years to a couple of gigayears. As for the COSMOS quenched sources, we place those from the HRS sample on the MS diagram (Fig. 8) to

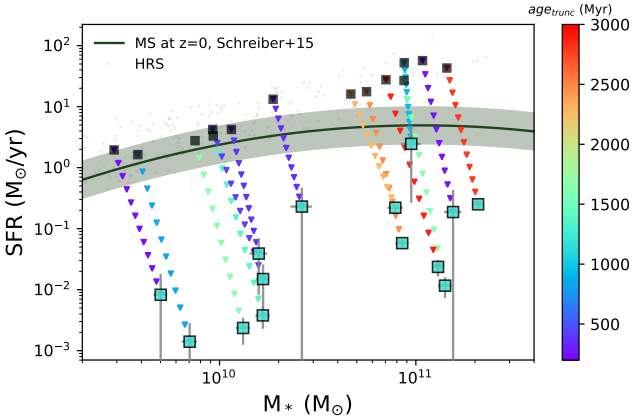

Fig. 8. Star formation rate as a function of stellar mass for the HRS galaxies. Grey dots represent late-type HRS galaxies. Squares show the HRS quenched sources studies in this work; their position relative to the star-forming MS of galaxies before their quenching is marked by grey symbols. Their evolution since quenching is indicated by the triangles coloured according to their $\rm age_{trunc}$. For comparison, the MS of Schreiber et al. (2015) at $z = 0$ is shown as a solid black line along with its dispersion (shaded grey region).

recover their position before quenching. This comparison shows that the HRS quenched sources are compatible with the $z = 0$ MS of Schreiber et al. (2015). The galaxies with the larger values of $\rm age_{trunc}$ (larger than a couple of gigayears) are the most massive sources.

We show the $L_{\rm IR}^{\rm now}/L_{\rm IR}^{\rm bq}$ ratio, that is, is the current $L_{\rm IR}$ and the one before quenching, respectively, as a function of $\rm age_{trunc}$ in Fig. 9 for all the HRS+COSMOS quenched galaxies. The two samples are complementary as the COSMOS galaxies probe shorter $\rm age_{trunc}$ compared to the local galaxies complementing the dynamical range in $\rm age_{trunc}$. To interpret the position of the sources on this diagram, we add tracks assuming an exponential decrease of the $L_{\rm IR}^{\rm now}/L_{\rm IR}^{\rm bq}$ ratio as a function of time after quenching assuming different e-folding times τ (from 50 to 1000 Myr). The position of the COSMOS galaxies, despite their large errors

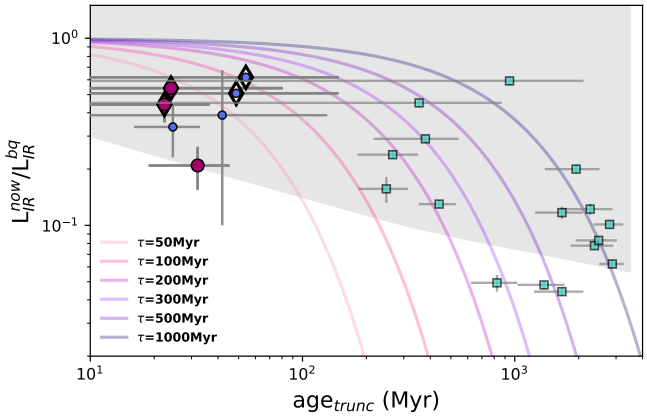

Fig. 9. Ratio between the observed $L_{\rm IR}$ and the $L_{\rm IR}$ before the truncation of the SFH as a function of the age of truncation of the SFH ($\rm age_{trunc}$). Circles are galaxies from the COSMOS quenched sample, the red ones are galaxies confirmed from their spectra. Diamonds indicate galaxies for which IR data are available. Cyan squares are galaxies from the local HRS quenched galaxies. The light grey shaded region indicates the region covered by the UV–NIR SED models used to determine the physical properties of the galaxies. The coloured tracks indicate an exponential decrease in $L_{\rm IR}^{\rm now}/L_{\rm IR}^{\rm bq}$ as a function of $\rm age_{trunc}$ assuming different e-folding times.

on the $\rm age_{trunc}$ is compatible with a decrease with a short e-folding time that is less than 300 Myr. Of the 14 HRS quenched galaxies, 5 are also compatible with these short τ values of a couple of hundred million years. Two HRS galaxies have very uncertain $\rm age_{trunc}$ estimates, which prevents us from discussing their position on the diagram. However, the positions of the other HRS quenched galaxies are compatible with a decrease over a longer timescale; seven of them are lying on the track of a decrease with an e-folding time of 1 Gyr. This is consistent with the physical process that caused their star formation quenching, namely ram pressure stripping due to the environment of the Virgo cluster. The positions of the COSMOS quenched sources on Fig. 9 imply a rapid and drastic physical process. Six out of the seven candidates seem to be compatible with a process linked to short timescales of less than ~100 Myr. Fluctuations in star formation on this timescale can be due to the formation and destruction of individual giant molecular clouds where feedback is locally too weak to prevent gravitational collapse (e.g., Scalo & Struck-Marcell 1984; Faucher-Giguère 2018; Orr et al. 2019; Tacchella et al. 2020, and references therein). However, the errors on $\rm age_{trunc}$ make the processes compatible with longer timescales of the order of a few hundred million years. Within this time range, star formation can be affected by galaxy mergers, bar-induced inflows, disk instabilities, galactic winds, and environmental effects (Gunn & Gott 1972; Hernquist 1989; Mihos & Hernquist 1996; Robertson et al. 2006; Oppenheimer & Davé 2008; McQuinn et al. 2010; Dekel & Burkert 2014; Zolotov et al. 2015; Tacchella et al. 2016, 2020; Sparre et al. 2017; Torrey et al. 2018; Wang et al. 2019). Further investigation of each of the COSMOS candidates is needed to identify the process responsible for the observed decrease in star formation activity.

7. Discussion

In the previous section, we show evidence for a decrease in the IR luminosity on different timescales but we have not put constraints on the origin of the decrease. It could be due to the absence of young stars heating the dust, and a lack of dust content may also contribute.

In Fig. 10, we compare the SFR and $L_{\rm IR}$ of the HRS+COSMOS galaxies obtained by the SED modelling of the UV-IR emission with CIGALE and compare their position with respect to the Kennicutt & Evans (2012) relation. All the sources are more than a factor of three below the relation. COSMOS sources with a 24 μm detection show the same departure from the Kennicutt & Evans (2012) relation with $L_{\rm IR}$. The departure from the relation is stronger for the HRS galaxies which are all a factor of ten below it. For the HRS galaxies, with IR decreasing timescales of the order of a few hundreds of Myr to a Gyr, this departure could imply that the IR luminosity is no longer connected to the recent star formation activity and is due to the contribution of the old stellar component. However, for the COSMOS galaxies and the very short $\rm age_{trunc}$ values obtained with CIGALE, and bearing in mind that CIGALE tends to overestimate them (see Fig. 3), it is possible that we are probing an evolutionary phase very close in time to the quenching process itself and that the $L_{\rm IR}$ due to the heating by young stars is starting to decrease. However, for these galaxies a contribution from the dust heated by evolved stellar populations is also expected and can explain the departure from the Kennicutt & Evans (2012) relation.

To investigate the contribution to dust heating by the evolved stellar population we show in Fig. 11 the $L_{\rm IR}/M_*$ ratio as a function of stellar mass for our candidates from both HRS and COSMOS. In addition, we show the $L_{\rm IR}/M_*$ ratio of HRS elliptical galaxies (see Boselli et al. 2010a, for the morphology details). We used their IR data from Smith et al. (2012) and Ciesla et al. (2012) and the stellar masses from Boselli et al. (2010a). These sources have no star formation activity and therefore their IR luminosity is due to the dust heating from old stars, or a strong radio AGN (Smith et al. 2012; Ciesla et al. 2012; Gomez et al. 2010; Boselli et al. 2010b). As show in Fig. 11, the $L_{\rm IR}/M_*$ ratio of our HRS quenched candidates is one to two orders of magnitude higher than the typical $L_{\rm IR}/M_*$ ratio of elliptical galaxies. For the COSMOS galaxies, the difference is stronger, with a difference in the $L_{\rm IR}/M_*$ ratio between the HRS elliptical galaxies and the COSMOS galaxies of at least two orders of magnitude. This implies that the IR luminosity that we observe and estimate for our quenched candidates cannot be solely due to heating from evolved stellar populations. Although this test rules out the possibility that the $L_{\rm IR}$ comes mainly from dust heated by evolved stellar populations, it does not assess the case of intermediate-age stars which can dominate the dust heating (see e.g., Utomo et al. 2014; Hayward et al. 2014). To estimate the contribution of intermediate-age stars in the $L_{\rm IR}$ of COSMOS quenched candidates, we use the SFH obtained from the best fit of each quenched galaxy to quantify the fraction of $L_{\rm IR}$ due to stars in different bins of age using the SED simulation function of CIGALE. The results are shown in Fig. 12 for different stellar age bins (0–10, 10–100, 100–500, 500–1000 Myr). On average, the contribution of 10–100 Myr stars to the total $L_{\rm IR}$ is 40% while the contribution of intermediate-age stars (with ages between 100 and 500 Myr) is on average 20–25%. Despite the recent rapid quenching, the fraction of young stars contributing to the $L_{\rm IR}$ is still significant.

The HRS quenched galaxies have been well sampled for their IR SED from mid-infrared (MIR) to submm (ten flux densities), allowing us to measure dust temperatures and dust masses from the SED fitting of the IR range only. To further our analysis, we measure those parameters for our quenched candidates. Indeed, the effect of ram pressure stripping is the quenching of

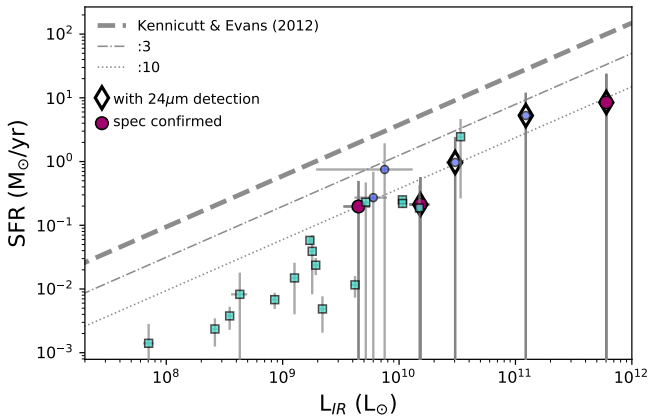

Fig. 10. SFR as a function of IR luminosity for the galaxies of the final sample obtained from the UV-submm SED fitting. Circles are galaxies from the final COSMOS sample, the red ones are galaxies confirmed from their spectra. Diamonds indicate galaxies for which IR data are available and well fitted. The dark purple dashed line shows the Kennicutt & Evans (2012) relation for normal star-forming galaxies.

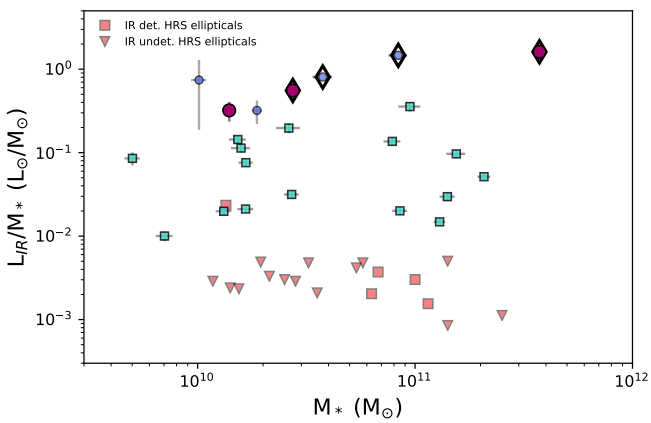

Fig. 11. Infrared-luminosity-to-stellar-mass ratio as a function of stellar mass for the candidate galaxies from both COSMOS and HRS (circles and squares, respectively). In red we show the positions of the HRS elliptical galaxies: IR detected (red squares) and IR undetected (red triangles).

star formation due to the removal of the gas from the galaxy. The HRS galaxies have a quenching age ranging from 100 to 3000 Myr which is a typical timescale for ram pressure stripping. Over several hundred million years, the young stars no longer heat the dust and therefore the decrease in $L_{\rm IR}$ is expected. There have been observations of dust-truncated profiles in galaxies undergoing ram pressure stripping (e.g., Boselli & Gavazzi 2006; Cortese et al. 2010, 2014; Longobardi et al. 2020). For each of our selected HRS galaxies, we computed the average dust mass of the reference samples of normal star-forming HRS galaxies with the same stellar mass as our selected quenched galaxies. For each of these sources, we then calculate the ratio between their dust mass and the average dust mass of their reference sample. In Fig. 13 (left panel), we show the $L_{\rm IR}^{\rm now}/L_{\rm IR}^{\rm bq}$ ratio as a function of the normalised dust mass. A weak trend is seen, but it is clear that they show a deficit in dust content with half of the candidates having a dust mass corresponding to less than 50% of the dust content of normal galaxies with similar stellar mass. This result is consistent with the fact that the quenched HRS galaxies have lower attenuation than normal star-forming galaxies of corresponding stellar masses, as shown

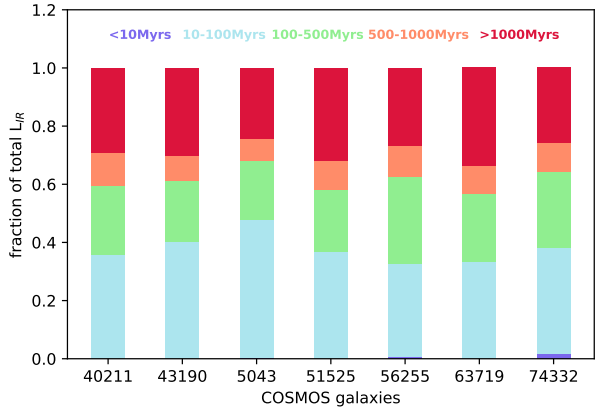

Fig. 12. Contributions of several stellar populations to the total $L_{\rm IR}$ for each of the seven quenched COSMOS galaxies.

in Fig. 13 (middle panel). There is a clear trend between $L_{\rm IR}^{\rm now}/L_{\rm IR}^{\rm bq}$ and the normalised V band attenuation. Quenched galaxies with the higher/lower deficit in attenuation compared to their reference sample are those with the lower/higher $L_{\rm IR}^{\rm now}/L_{\rm IR}^{\rm bq}$ ratio, respectively. We also computed a 'normalized' dust temperature for each quenched galaxy using the same reference sample but found no trend. The normalised dust temperature showed the same value for each quenched galaxy but with a large error which prevents us from coming to any robust conclusions as to the effect on the heating process. Either the dynamical range probed by the HRS in terms of dust temperature is not sufficient to see any trend, or there is no lower dust temperature in quenched galaxies compared to their reference sample. Therefore, understanding the decrease in $L_{\rm IR}$ is difficult as it can be attributed to both a lack of young stars heating the dust and a deficit in dust content. Finally, in Fig. 13 (right panel) we show the normalised $M_{\rm dust}$ as a function of the normalised V band attenuation. Although weak, there is a trend that confirms a link between the lack of dust and the low V band attenuation in the HRS quenched galaxies. A similar investigation would be needed to understand the origin of the star formation quenching of the COSMOS quenched sources, but a better IR sampling of their SED and/or probes of their gas content would be needed to perform such an analysis.

8. Conclusions

We investigate the IR luminosity decrease in galaxies after quenching of their star formation activity. First, we used a sample of local well-known galaxies, the *Herschel* Reference Survey by selecting 14 galaxies that experienced rapid and drastic quenching of their star formation activity (more than 99%) in the last gigayear. These galaxies are members of the Virgo cluster and are known to have undergone ram pressure stripping. In addition, we selected galaxies at higher ($0.5 < z < 1$) redshift in the COSMOS field. We rely on the statistical work of Aufort et al. (2020) who provide the probabilities for individual members of a subsample of COSMOS galaxies to have undergone a rapid and recent variation of their SFH. We selected seven sources using the exact same criteria as for the HRS galaxies, that is, a decrease in the SFR by more than 99%.

We performed UV-to-IR SED modelling of the HRS+COSMOS sources to estimate the age of the quenching and the $L_{\rm IR}$ of the galaxies. For the HRS galaxies, an IR-only SED modelling was performed to estimate the present $L_{\rm IR}$ of

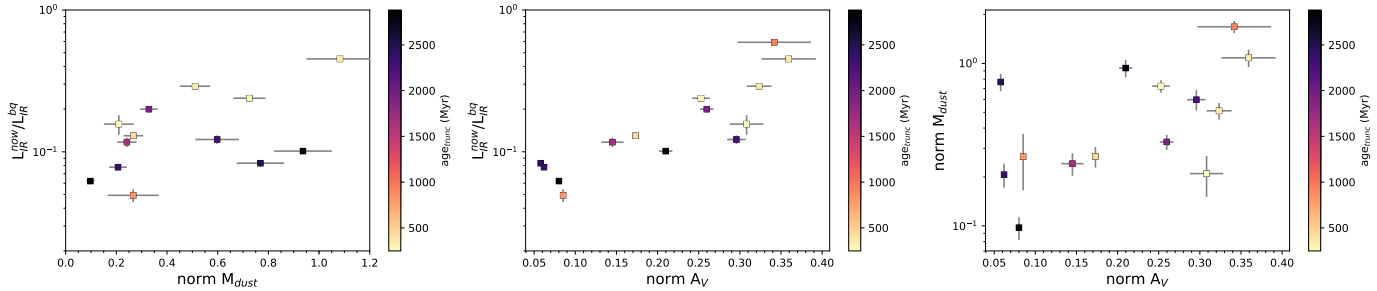

Fig. 13. Normalised physical properties of the HRS quenched galaxies as a function of $L_{\rm IR}^{\rm now}/L_{\rm IR}^{\rm bq}$. These are the dust mass (*left panel*), the dust temperature (*middle panel*), and the FUV attenuation (*right panel*) normalised by the corresponding property of a reference sample built to have the same stellar mass as the quenched source. Symbols are colour-coded according to their age of quenching age$_{\rm trunc}$.

the galaxies. We validated our estimate of the age of quenching with the results of Boselli et al. (2016) who used spectroscopy in addition to photometry and performed a detailed and more specific analysis of these sources. For the COSMOS galaxies, we used the measurement of the present $L_{\rm IR}$ provided by the UV-to-IR SED modelling by CIGALE and checked its validity in cases where an IR data point is absent.

For both the HRS and COSMOS quenched galaxies, we estimate the $L_{\rm IR}$ immediately before quenching took place using the SED of each quenched source at the moment immediately before quenching. We obtained the past $L_{\rm IR}$ of these galaxies and find that it is consistent with the $L_{\rm IR}$ of a reference sample built for each quenched galaxy to be similar in stellar mass and normally forming stars. We conclude that our method is able to recover the past properties of galaxies, with the caveat that the more recent the quenching, the higher the precision on the estimated past $L_{\rm IR}$.

Gathering the local and high-redshift samples, we investigated the relation between the ratio of observed $L_{\rm IR}$ to $L_{\rm IR}$ before quenching and the quenching age in order to put a constraint on the timescales of the decrease in the IR luminosity after the shutdown of star formation. Assuming an exponential decrease in the $L_{\rm IR}$ after quenching, we find that the COSMOS quenched galaxies have typical timescales that are short, that is, of less than a few million years while the HRS quenched galaxies are consistent with a decrease with an e-folding time of several hundred million years up to 1 Gyr. For the HRS quenched galaxies, this is consistent with their known quenching process which is ram pressure stripping due to the environment of the Virgo cluster. The differences between the HRS and the COSMOS quenched galaxies in terms of age$_{\rm trunc}$ and the timescale over which $L_{\rm IR}$ decreases suggest different quenching processes.

A comparison between the $L_{\rm IR}/M_*$ ratios of our HRS and COSMOS selected galaxies and those of HRS elliptical galaxies with no more star formation activity shows that the IR emission of our candidates cannot be solely due to dust heating from evolved stellar populations and that young stars still contribute ~40% of the total $L_{\rm IR}$. Also, we clearly see a deficit in dust mass in the HRS galaxies, which is in agreement with the lower attenuation in the V band for the quenched galaxies. This is expected because we know that these galaxies suffer from ram pressure stripping, which affects the dust content as well. However, no conclusions can be drawn for the dust temperature because we see no clear difference between the average dust temperature of the quenched candidates and that of their reference sample. In other words, further characterisation of the decrease in IR luminosity is challenging and will require more time-sensitive indicators such as IR emission lines. Probing the dust content of the COSMOS sample would allow stronger constraints to be placed on the present IR luminosity and would allow further analysis of the dust content of these sources.

Acknowledgements. L. C. warmly thanks Emanuele Daddi for useful comments that really improved the paper and Mauro Giavalisco for an interesting discussion in Sesto that gave the idea of this study. The project has received funding from Excellence Initiative of Aix-Marseille University - AMIDEX, a French Investissements dAvenir programme.

References

Aufort, G., Ciesla, L., Pudlo, P., & Buat, V. 2020, A&A, 635, A136
Battisti, A. J., Cunha, E. d., Shivaei, I., & Calzetti, D. 2020, ApJ, 888, 108
Bendo, G. J., Galliano, F., & Madden, S. C. 2012, MNRAS, 423, 197
Blank, M., Meier, L. E., Macciò, A. V., et al. 2021, MNRAS, 500, 1414
Boissier, S., & Prantzos, N. 2000, MNRAS, 312, 398
Boquien, M., Buat, V., & Perret, V. 2014, A&A, 571, A72
Boquien, M., Burgarella, D., Roehlly, Y., et al. 2019, A&A, 622, A103
Boselli, A., & Gavazzi, G. 2006, PASP, 118, 517
Boselli, A., Boissier, S., Cortese, L., et al. 2006, ApJ, 651, 811
Boselli, A., Eales, S., Cortese, L., et al. 2010a, PASP, 122, 261
Boselli, A., Ciesla, L., Buat, V., et al. 2010b, A&A, 518, L61
Boselli, A., Hughes, T. M., Cortese, L., Gavazzi, G., & Buat, V. 2013, A&A, 550, A114
Boselli, A., Cortese, L., & Boquien, M. 2014a, A&A, 564, A65
Boselli, A., Cortese, L., Boquien, M., et al. 2014b, A&A, 564, A67
Boselli, A., Fossati, M., Gavazzi, G., et al. 2015, A&A, 579, A102
Boselli, A., Roehlly, Y., Fossati, M., et al. 2016, A&A, 596, A11
Boselli, A., Lupi, A., Epinat, B., et al. 2021, A&A, 646, A139
Bruzual, G., & Charlot, S. 2003, MNRAS, 344, 1000
Buat, V., Noll, S., Burgarella, D., et al. 2012, A&A, 545, A141
Buat, V., Heinis, S., Boquien, M., et al. 2014, A&A, 561, A39
Buat, V., Ciesla, L., Boquien, M., Małek, K., & Burgarella, D. 2019, A&A, 632, A79
Charlot, S., & Fall, S. M. 2000, ApJ, 539, 718
Chen, T., & Guestrin, C. 2016, in Proceedings of the 22nd ACM SIGKDD International Conference on Knowledge Discovery and Data Mining (ACM), 785
Ciesla, L., Boselli, A., Smith, M. W. L., et al. 2012, A&A, 543, A161
Ciesla, L., Boquien, M., Boselli, A., et al. 2014, A&A, 565, A128
Ciesla, L., Charmandaris, V., Georgakakis, A., et al. 2015, A&A, 576, A10
Ciesla, L., Boselli, A., Elbaz, D., et al. 2016, A&A, 585, A43
Ciesla, L., Elbaz, D., & Fensch, J. 2017, A&A, 608, A41
Ciesla, L., Elbaz, D., Schreiber, C., Daddi, E., & Wang, T. 2018, A&A, 615, A61
Cortese, L., Davies, J. I., Pohlen, M., et al. 2010, A&A, 518, L49
Cortese, L., Boissier, S., Boselli, A., et al. 2012, A&A, 544, A101
Cortese, L., Fritz, J., Bianchi, S., et al. 2014, MNRAS, 440, 942
Daddi, E., Dickinson, M., Morrison, G., et al. 2007, ApJ, 670, 156
Dale, D. A., Helou, G., Magdis, G. E., et al. 2014, ApJ, 784, 83
Dekel, A., & Burkert, A. 2014, MNRAS, 438, 1870
Durret, F., Chiche, S., Lobo, C., & Jauzac, M. 2021, A&A, 648, A63
Elbaz, D., Daddi, E., Le Borgne, D., et al. 2007, A&A, 468, 33
Elbaz, D., Dickinson, M., Hwang, H. S., et al. 2011, A&A, 533, A119
Elbaz, D., Leiton, R., Nagar, N., et al. 2018, A&A, 616, A110
Faucher-Giguère, C.-A. 2018, MNRAS, 473, 3717
Förster Schreiber, N. M., & Wuyts, S. 2020, ARA&A, 58, 661
Fumagalli, M., Krumholz, M. R., Prochaska, J. X., Gavazzi, G., & Boselli, A. 2009, ApJ, 697, 1811

Gavazzi, G., Pierini, D., & Boselli, A. 1996, A&A, 312, 397
Gavazzi, G., Consolandi, G., Dotti, M., et al. 2015, A&A, 580, A116
Giovannoli, E., Buat, V., Noll, S., Burgarella, D., & Magnelli, B. 2011, A&A, 525, A150
Gomez, H. L., Baes, M., Cortese, L., et al. 2010, A&A, 518, L45
Gunn, J. E., & Gott, J. R., III 1972, ApJ, 176, 1
Guo, K., Zheng, X. Z., & Fu, H. 2013, ApJ, 778, 23
Hayward, C. C., Lanz, L., Ashby, M. L. N., et al. 2014, MNRAS, 445, 1598
Hernquist, L. 1989, Nature, 340, 687
Ilbert, O., Arnouts, S., Le Floc'h, E., et al. 2015, A&A, 579, A2
Jin, S., Daddi, E., Liu, D., et al. 2018, ApJ, 864, 56
Kennicutt, R. C., & Evans, N. J. 2012, ARA&A, 50, 531
Laigle, C., McCracken, H. J., Ilbert, O., et al. 2016, ApJS, 224, 24
Lilly, S. J., Le Brun, V., Maier, C., et al. 2009, ApJS, 184, 218
Longobardi, A., Boselli, A., Boissier, S., et al. 2020, A&A, 633, L7
Magdis, G. E., Daddi, E., Béthermin, M., et al. 2012, ApJ, 760, 6
Małek, K., Buat, V., Roehlly, Y., et al. 2018, A&A, 620, A50
Marin, J.-M., Pudlo, P., Robert, C. P., & Ryder, R. J. 2012, Stat. Comput., 22, 1167
Matthee, J., & Schaye, J. 2019, MNRAS, 484, 915
McQuinn, K. B. W., Skillman, E. D., Cannon, J. M., et al. 2010, ApJ, 721, 297
Mihos, J. C., & Hernquist, L. 1996, ApJ, 464, 641
Noeske, K. G., Weiner, B. J., Faber, S. M., et al. 2007, ApJ, 660, L43
Noll, S., Burgarella, D., Giovannoli, E., et al. 2009, A&A, 507, 1793
Oppenheimer, B. D., & Davé, R. 2008, MNRAS, 387, 577
Orr, M. E., Hayward, C. C., & Hopkins, P. F. 2019, MNRAS, 486, 4724
Pannella, M., Carilli, C. L., Daddi, E., et al. 2009, ApJ, 698, L116
Pforr, J., Maraston, C., & Tonini, C. 2012, MNRAS, 422, 3285
Querejeta, M., Meidt, S. E., Schinnerer, E., et al. 2015, ApJS, 219, 5
Robert, C. 2007, The Bayesian Choice: From Decision Theoretic Foundations to Computational Implementation (Springer Science & Business Media)
Robertson, B., Bullock, J. S., Cox, T. J., et al. 2006, ApJ, 645, 986
Rodighiero, G., Daddi, E., Baronchelli, I., et al. 2011, ApJ, 739, L40
Salmi, F., Daddi, E., Elbaz, D., et al. 2012, ApJ, 754, L14
Salpeter, E. E. 1955, ApJ, 121, 161
Sargent, M. T., Daddi, E., Béthermin, M., et al. 2014, ApJ, 793, 19
Scalo, J. M., & Struck-Marcell, C. 1984, ApJ, 276, 60
Schreiber, C., Pannella, M., Elbaz, D., et al. 2015, A&A, 575, A74
Schreiber, C., Pannella, M., Leiton, R., et al. 2017, A&A, 599, A134
Scoville, N., Sheth, K., Aussel, H., et al. 2016, ApJ, 820, 83
Sisson, S. A., Fan, Y., & Beaumont, M. 2018, Handbook of Approximate Bayesian Computation (Chapman and Hall/CRC)
Smith, M. W. L., Gomez, H. L., Eales, S. A., et al. 2012, ApJ, 748, 123
Sparre, M., Hayward, C. C., Feldmann, R., et al. 2017, MNRAS, 466, 88
Speagle, J. S., Steinhardt, C. L., Capak, P. L., & Silverman, J. D. 2014, ApJS, 214, 15
Tacchella, S., Dekel, A., Carollo, C. M., et al. 2016, MNRAS, 458, 242
Tacchella, S., Forbes, J. C., & Caplar, N. 2020, MNRAS, 497, 698
Tomczak, A. R., Quadri, R. F., Tran, K.-V. H., et al. 2016, ApJ, 817, 118
Torrey, P., Vogelsberger, M., Hernquist, L., et al. 2018, MNRAS, 477, L16
Utomo, D., Kriek, M., Labbé, I., Conroy, C., & Fumagalli, M. 2014, ApJ, 783, L30
Vaccari, M. 2016, in The Universe of Digital Sky Surveys, eds. N. R. Napolitano, G. Longo, M. Marconi, M. Paolillo, & E. Iodice, 42, 71
Wang, E., Lilly, S. J., Pezzulli, G., & Matthee, J. 2019, ApJ, 877, 132
Whitaker, K. E., Franx, M., Leja, J., et al. 2014, ApJ, 795, 104
Wuyts, S., Förster Schreiber, N. M., van der Wel, A., et al. 2011, ApJ, 742, 96
Zolotov, A., Dekel, A., Mandelker, N., et al. 2015, MNRAS, 450, 2327

Appendix A: Optical spectra of the candidates

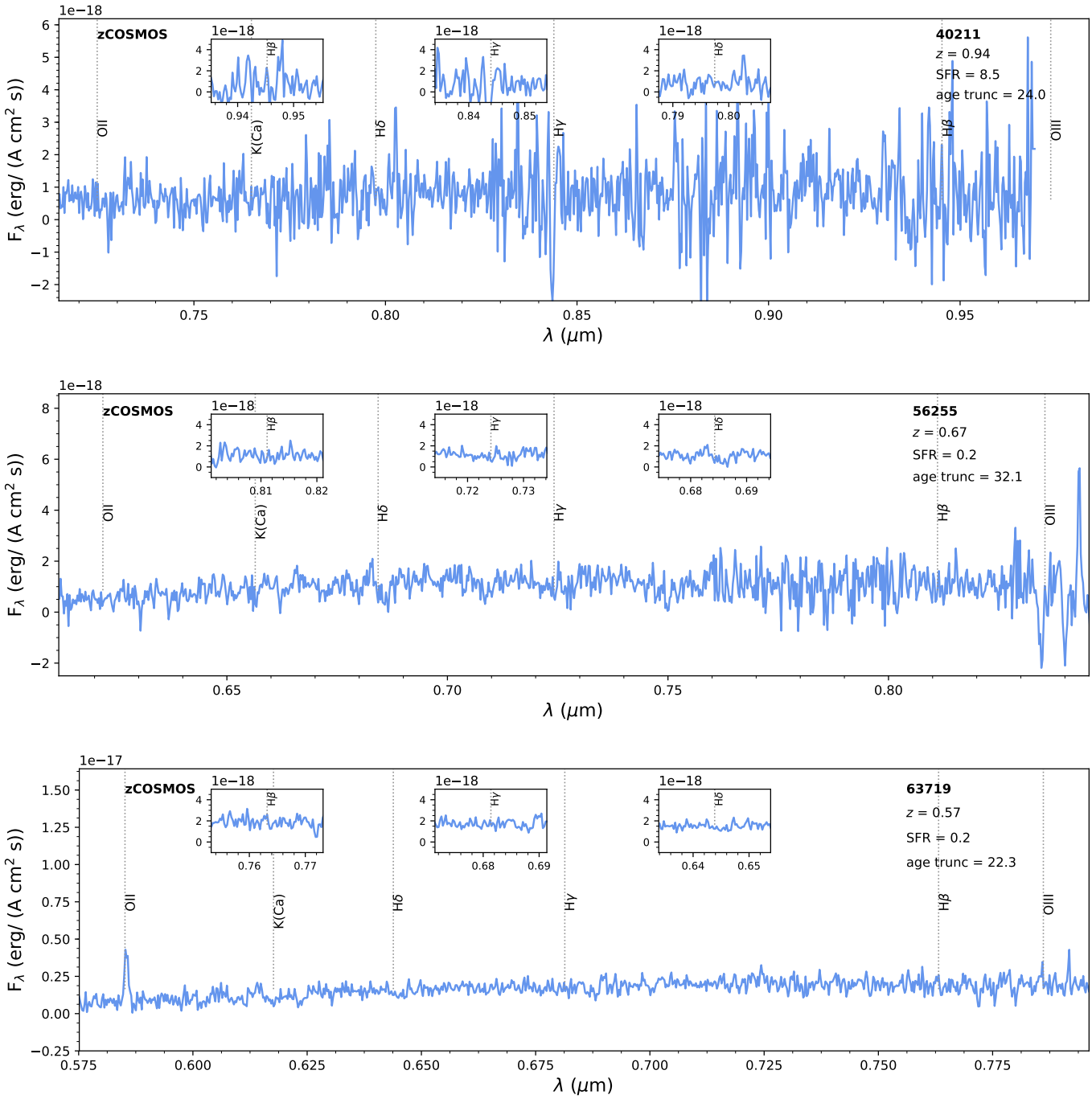

Fig. A.1. zCOSMOS spectra for galaxies of the final sample where available. Inset panels are zooms onto on the Hβ, Hγ, and Hδ lines.